Arabian Journal of Chemistry (2022) **15**, 104074

King Saud University

Arabian Journal of Chemistry

www.ksu.edu.sa
www.sciencedirect.com

ORIGINAL ARTICLE

Evaluation of the effect of Si/Mo and oil/alcohol ratios in the production of biodiesel from soybean oil

Raquel K.P. Cardoso, Gabriel V.A. Silva, Bruno T.S. Alves, Vitória A. Freire, José J.N. Alves, Bianca V.S. Barbosa *

Catalysis, Characterization and Biofuels Laboratory, Department of Chemical Engineering, Federal University of Campina Grande, 58429-900 Campina Grande, Paraíba, Brazil

Received 7 March 2022; accepted 22 June 2022
Available online 27 June 2022

KEYWORDS

Heterogeneous catalyst;
Transesterification;
KIT-6;
Biodiesel;
Molybdenum

Abstract Mo-KIT-6 catalysts precursors obtained by direct hydrothermal synthesis using different Si/Mo molar ratios (10, 20, 30) were evaluated in the production of biodiesel from the transesterification of soybean oil with methanol. A 2^2 + 3PtCt factorial design was used to evaluate the influence of alcohol/oil and Si/Mo ratios on biodiesel yield. ANOVA statistical analysis showed that Si/Mo ratio was the most significant variable. The factorial design showed that the optimal conditions for maximizing the biodiesel yield are: using the 10_Mo-KIT-6 catalyst, and an alcohol/oil ratio of 20/1 at 150 °C for 3 h. However, using the 20_Mo-KIT-6 catalyst with an alcohol/oil ratio of 15/1 the biodiesel yield is close to the maximum, having the advantage of using a lower amount of methanol, which means that the separation of non-reacted alcohol will consume less energy.

1. Introduction

Energetic demand has been continuously increasing due to population growth, modernization and industrial expansion. The majority of energy sources comes from non-renewable sources such as fossil fuels, mineral coal, oil and natural gas (Dantas et al., 2020). Oil based fossil diesel has been the main energy source for conventional diesel engines for many decades. However, fuels derived from these sources are the ones which most contribute to environmental pollution (Krishnasamy and Bukkarapu, 2021). In order to achieve sustainable economic growth, it becomes necessary to reduce harmful impacts caused by current predominant energy sources by developing new technologies for production of renewable and efficient energies. Increasing concerns about the environment, as well as energy security considerations, have motivated the scientific community to investigate a viable replacement for fossil diesel.

The possibility of using vegetable oils as fuel has been recognized since the inception of diesel engines. However, fuels from this type of biomass are not competitive with oil as they are more expensive (Hosseinzadeh-Bandbafha et al., 2018). The factors that contribute to the high cost of this fuel are the geographical area, the variability

* Corresponding author at: UFCG/CCT/UAEQ, Aprígio Veloso Avenue 882, Bodocongó, Campina Grande, Paraíba CEP 58109-970, Brazil.
E-mail address: bianca.viana@eq.ufcg.edu.br (B.V.S. Barbosa).
Peer review under responsibility of King Saud University.

Production and hosting by Elsevier

https://doi.org/10.1016/j.arabjc.2022.104074
1878-5352

of agricultural production that varies from season to season, the price of crude oil, with energy efficiency and raw material being the most onerous factors (Chuah et al., 2016).

Among biofuels, biodiesel is a renewable alternative that has been identified as versatile fuel for diesel engines applications. It is miscible with diesel in any proportion, and requires no major engine modifications (Hosseinzadeh-Bandbafha et al., 2018). Favorable properties, such as renewability, biodegradability, non-toxicity and reduced sulphur oxide (SOx) and greenhouse gas enable biodiesel contributes towards environmental protection (Chuah et al., 2016; Wong et al., 2019). The production and use of biofuels from locally available biomass offer energy security, agricultural development, and job opportunities (Ewunie et al., 2021), as well as decreases dependence on oil imports (Manojkumar et al., 2020).

Industrially, the most widely used method for producing biodiesel is alcoholic transesterification in the presence of homogeneous catalysts (Moraes et al., 2020). The reaction is reversible and various factors such as methanol/oil ratio, catalyst content, temperature, and contact time are cost effective on the biodiesel production (Zhang et al., 2022).

The transesterification reaction consists of the reaction between a triglyceride and a primary monoalcohol, usually methanol, in the presence of a homogeneous catalyst, such as potassium hydroxide (KOH) or sodium hydroxide (NaOH), producing a mixture of fatty acid esters and glycerol as co-product (Rezania et al., 2019; Athar and Zaidi, 2020).

The homogeneous catalysts used in the process present some disadvantages: high costs of the process of catalyst separation; generation of high amounts of waste water during products purification; susceptible to soap formation from water and fatty acids in reacting system (Luna et al., 2017). The catalyst is not completely recovered being partially consumed in the process. An alternative for the improvement and reduction of process costs is the use of heterogeneous catalysts that facilitates the purification of alkyl mono-esters, allows the recovery and regeneration of the solid catalyst over its lifetime, and facilitates the recovery and purification of glycerin (Orege et al., 2022). Many solids have been studied and developed as potential catalysts for biodiesel synthesis. The solid catalysts performance is related to the nature of their acid or basic sites (Zabeti et al., 2009).

Metal catalysts supported on mesoporous molecular sieves have been widely used in petrochemical industries (Li et al., 2020a; Faba et al., 2020). The molecular sieve KIT-6 is a material made of mesoporous silica formed by a system of bi-continual tridimensional networks and interpenetrating canals which favor direct contact and provide open access of guest molecules without pore blocking that might be adjustable to the range of 4–12 nm (Kleitz et al., 2007, 2003). This sieve is used as a support for transition metal ions. The crystalline, textural and morphological properties contribute to dispersion of the metal active sites that influence catalytic performance (Liu et al., 2016).

Molybdenum trioxide is an example of an active material that can be incorporated into the KIT-6 molecular sieve. The catalytic performance of Mo-KIT-6 catalysts has been evaluated for different reactions: olefin metathesis (Uchagawkar et al., 2020), epoxidation (Bigi et al., 2014), hydrodesulfurization (Ali and Saleh, 2020), hydroformylation (Sakthivel et al., 2015) and chemical processes of photo-oxidation (Young, 2003). Molybdenum catalysts are associated with reduction and oxidation processes. The high oxidation state of this type of metal can provide its acting as both Lewis and Bronsted-Lowry acid sites. Such property theoretically enables their use in the transesterification reaction (Silva et al., 2018), which is the objective in this work.

Arrais Gonçalves et al. (2021) synthesized a $SrFe_2O_4$ with 35 wt% MoO_3 catalyst, calcined at 450 °C for 2 h, for biodiesel production. This catalyst was evaluated for transesterification of waste cooking oil using a face-centered central composite design 2^4. The maximum yield of biodiesel was obtained at 164 °C, oil/alcohol molar ratio of 1/40, 10 wt% of catalyst and 4 h of reaction.

Pinto et al. (2019) produced MoO_3 catalysts using different calcination temperatures. The maximum yield of methyl esters was 94.8% obtained in the presence of the catalyst calcined at 600 °C under the optimized reaction conditions of oil/alcohol molar ratio of 1/45, 0.5 wt% catalyst, at 150 °C for 4 h reaction.

Xie and Zhao (2014) synthesized heterogeneous CaO-MoO_3/SBA-15 catalysts and evaluated its performance in the soybean oil transesterification reaction from different conditions of oil/alcohol molar ratio, reaction time and catalyst loading. The maximum biodiesel yield of 83.2% was obtained with the solid catalyst with 40 wt% of CaO-MoO_3 calcined at 550 °C at the following conditions: 50 h of reaction, 6 wt% of catalyst, an oil/methanol molar ratio of 1/50, and temperature of 65 °C.

Achievement of maximum biodiesel yield is the ultimate goal of the production unit, and that can be attained by optimizing the transesterification process conditions. In this work the objective was to evaluate the catalytic performance of a new heterogeneous catalyst in the transesterification reaction for biodiesel production. The catalyst was obtained by incorporating molybdenum into the structure of KIT-6 by direct synthesis with different Si/Mo molar ratios (10, 20, 30). Its performance was evaluate for soybean oil transesterification via methyl route. A factorial design of experiment 2^2 with 3 central points was used to evaluate the effect of molybdenum concentration and alcohol/oil ratio on biodiesel yield.

2. Mechanism of reaction

The mechanism of reaction of the heterogeneous process of biodiesel production follows the classical steps of heterogeneous reaction: (1) external diffusion of reactants, (2) intraparticle diffusion, (3) adsorption of reactants at catalyst surface, (4) reaction, (5) desorption of products, (6) intraparticle diffusion of products, and (7) external diffusion of products. External diffusion can easily be eliminated by agitation, so steps 1 and 7 are eliminated. In a heterogeneous catalytic environment, intraparticle diffusion may be a big concern. To minimize the internal diffusion resistance, heterogeneous catalysts should have uniform distribution of pores and high surface area. Adsorption is a fundamental and essential step in the reaction of transesterification, and the catalyst must have the property hydrophobic surface. The existence of acidic or basic active sites are another requirement to accelerate the reactional step (Chooi et al., 2021). The reactivity can be adjusted by controlling the morphology (Mukhtar et al., 2022). Solids that have Lewis acid and/or basic sites are among the most tested as potential catalysts for biodiesel production (Cordeiro et al., 2011). Acidic catalysts provide positive charges on the active sites of the catalyst for the adsorption of fatty acids, while alkaline catalysts generate negative charges on the active sites for the adsorption of methanol. In the alkaline catalytic process, a tetrahedral intermediate is produced due to the reaction between alkoxide ion and alkyl group in the triglyceride, which reacts with the alcohol. In the acidic catalytic process, a carbocation is produced because a nucleophile attack creates a tetrahedral intermediate that removes glycerol, forming a new ester.

3. Experimental

3.1. Catalyst preparation

3.1.1. Direct synthesis of the x_Mo-KIT-6 catalyst

Catalysts (*x*_Mo-KIT-6) with Si/Mo molar ratios of 10, 20 and 30 were prepared following an adapted version of the methodology described by (Kleitz et al., 2003). Initially, the Pluronic triblock copolymer P_{123} was dissolved in deionized water with

hydrochloric acid (HCl, 37%) under stirring for 6 h at 35 °C. After this period, n-butanol (BuOH) was added to the solution. Afterwards, the silica source tetraethyl orthosilicate (TEOS) and the solution of ammonium molybdate tetrahydrate were simultaneously trickled into the original reactional mixture. The solution was kept under stirring for 24 h at 35 °C. The obtained gel was submitted to hydrothermal treatment in an oven for 24 h at 100 °C. The obtained material was washed until reaching pH = 7, and dried in a heating chamber for 24 h under 60 °C. The catalysts were activated by calcination, under a synthetic air flow for 6 h, having its temperature varied from room temperature of 25 °C up to 550 °C with a heating ramp of 5 °C min^{-1}.

3.2. Solids characterization

The thermogravimetric analysis was used to investigate the thermal stability of catalysts and decomposition temperature of the molybdenum salt. Thermogravimetric analyzes were performed using a TGA-51 Shimadzu Thermogravimetric Analyzer coupled to a computer (for data storage) by the TA-60 WS collection monitor software. The samples were subjected to a temperature variation of 30–1000 °C, with a heating rate of 5 °C min^{-1}, under a synthetic air flow rate of 50 mL min^{-1}.

The structural characteristics, identifications of phases and determination of crystallite size and crystallinity of the catalyst was investigated by using the X-ray diffraction method with a Shimadzu XRD-600 equipment, employing a Cu Kα radiation at 40 kV and 30 mA.

Fourier-transformed infrared (FTIR) spectra for the catalytic precursor and catalysts were obtained with a Spectrum 400 Perkin Elmer spectrophotometer. The analysis was performed out in the region from 4000 to 400 cm^{-1} wave number with a resolution of 4 cm^{-1} using a solid mixture with KBr.

Textural properties, pore volume and average pore size, and specific surface area of *x*_Mo-KIT-6 catalysts were evaluated from N_2 adsorption isotherms and BET method (Leofanti et al., 1998), using a Quantachrome gas adsorption analyzer, model 3200E YOUNG.

3.3. Biodiesel production

3.3.1. Experimental planning

A 2^2 + 3 CtPt factorial design was used to evaluate the influence of oil/alcohol molar ratio and Si/Mo ratio in the catalysts on the biodiesel yield in the transesterification reaction of soybean oil. Table 1 shows the experimental levels of the independent variables used in this study.

The effects of the oil/alcohol molar ration in the range of 1/10–1/20 and the Si/Mo ratio in the range of 10–30 were evaluated. An experimental design with 3 levels for both variables was used, with the central point being the average of the limits of the intervals.

Minitab 17.0® software was used to perform statistical analysis and regression of the data. Different models (linear and quadratic) were tested and analyzed based on Analysis of Variance (ANOVA). Eq. (1) describes the relationship between the dependent variable (Y) and the independent (X_n) uncoded variables, where a_n, a_{nn}, and a_{nm} are the linear regression coefficients.

$$Y = a_0 + \sum_{n=1}^{2} a_n X_n + \sum_{n=1}^{2} a_{nn} X_n{}^2 + \sum_{n=1}^{2} \sum_{m=n+1}^{2} a_{nm} X_n X_m \quad (1)$$

3.3.2. Transesterification reaction

KIT-6 catalysts with different Si/Mo molar ratios were used in the methyl transesterification reaction of soybean oil with different oil/alcohol ratios to evaluate the catalytic potential. The reaction was carried out in a batch reactor manufactured by Parr Instruments Inc. – Model 4848. The reactor is an autoclave made of stainless steel with a volume of 300 mL. The reactional system containing an oil and alcohol mixture with 3 wt% catalyst, was sealed and heated from room temperature to 150 °C, and stirred at 500 rpm for 3 h. After the reaction time, the catalyst and glycerin were separated from the products by filtration and decantation. Any trace of water was adsorbed from the product with anhydrous magnesium sulfate ($MgSO_{4(s)}$) and the phases solid and liquid separated by centrifugation.

3.4. Biodiesel characterization

The biodiesel or fatty acid methyl ester (FAME) content was determined following the standard method according to EN 14103 (Thoai et al., 2017), by using a Shimadzu GC 2010 Plus gas chromatograph with a split/splitless injector, a flame ionization detector (FID), an AOC-20i auto-injector, and a 100% dimethyl polysiloxane capillary column RTX-WAX 30 m × 0.32 mm × 0.25 μm (Restek Corporation). The operating conditions were as follows: FID temperature of 250 °C; initial column temperature of 210 °C; final column temperature of 250 °C; H_2 linear velocity of 50 cm s^{-1}; and split mode injection in the ratio of 1:50. Methyl heptadecanoate was used as the standard for GC-FID. Eq. (2) was used to determine the total fatty acid methyl esters content in the mixture biodiesel and non-reacted soybean oil, C_{FAME} (wt.%).

$$C_{FAME} = \frac{(S_A - A_{EI})}{A_{EI}} \times \frac{(C_{EI} \times V_{EI})}{m} \times 100\% \quad (2)$$

where, S_A represents sum of the peak areas, A_{EI} is the peak area of methyl heptadecanoate (internal standard), C_{EI} is the concentration (mg/mL) of methyl heptadecanoate solution (10 mg/mL), V_{EI} represents the volume (mL) of methyl heptadecanoate and 'm' is the mass (mg) of the FAME sample.

The individual FAMEi content in the biodiesel was calculate from Eq. (3).

$$C_{FAME_i} = \frac{(A_{FAME_i})}{A_{EI}} \times \frac{(C_{EI} \times V_{EI})}{m} \times 100\% \quad (3)$$

where,

C_{FAME_i} is the $FAME_i$ content (wt. %);
A_{FAME_i} is the $FAME_i$ area calculated by integration of the corresponding peaks in the chromatogram.

The specific mass data were determined following the standard established by EN ISO 3675/12185 and ASTM D1298 (Atabani et al., 2012), using a Density Master DMA 4100 M equipment. The biodiesel acidity index was determined by titration of the oil with a solution of ethyl ether and ethyl alco-

Table 1 Levels of independent variables in the experimental planning 2^2 + 3CtPt for evaluation of the transesterification of soybean oil.

Independent variable	Symbol	Levels		
		−1	0	+1
Oil/alcohol	A	1/10	1/15	1/20
Si/Mo	B	10	20	30

hol (2:1) using 0.1 M potassium hydroxide as the titrant, according to the methodology in ASTM D664 and EN 14104 standards (Sakthivel et al., 2018). (See Fig. 1).

4. Results and discussion

4.1. Characterization of the catalyst

4.1.1. Thermogravimetric analysis (TG/DTG)

Calcination temperature was determined from the thermogravimetric curve shown in Fig. 2. It may be observed two distinct temperature ranges, corresponding to two mass loss events. In the first event (I), in the temperature range of 22.84–152.38 °C, occurs a mass loss of 6.39%, which corresponds to desorption of physisorbed water and butane volatilization; in the second event (II), within the range of 152.38–548.54 °C , there is a mass loss of 43.71%, which is attributed to the non-ionic surfactant decomposition. After the mentioned last interval, thermogravimetric curve comes into equilibrium, indicating that the calcination temperature for complete removal of the organic driver is 550 °C.

4.1.2. X-ray diffraction analysis (XRD)

Fig. 3 shows the X-ray diffraction analysis of the KIT-6 molecular sieve and *x*_Mo-KIT-6 catalysts. It is possible to see the presence of two peaks, which correspond to characteristic reflections of orderly mesoporous cubic structure. The analysis in the Fig. 3 (a, b, c, d) presents reflection corresponding to Miller index (211) indicating the formation of *Ia3d* cubic structure; lower intensity peaks, corresponding to Miller indexes (220) and (332), indicate that the cubic structure presented organization at long reach of pores (Kleitz et al., 2007, 2003). However, 10_Mo-KIT-6 catalyst presented smaller organizational structure, since the reflection at (220) was not identified.

Fig. 4 shows the XRD analysis of *x*_Mo-KIT-6 catalysts with a scan angle of 2θ = 10 a 60°. From the analysis in Fig. 4 (a, b, c) it is observed that around 2θ = 23° the materials present an amorphous region which is characteristic of silica materials. In direct synthesis, metal atoms bond directly to the molecular sieve structure in such a way that the absence of metal characteristic peaks is an indicator that the Mo atoms replaced Si atoms in the crystal network of KIT-6 (Cabrera-munguia et al., 2017). The presence of molybdenum characteristic peaks was not identified in the XRD analysis.

Table 2 shows crystallographic parameters of the KIT-6 molecular sieve and the *x*_Mo-KIT-6 catalysts. It is observed that with the increase in molybdenum content incorporated on the structure of KIT-6 there is a shift towards the left of the peak referring to the reflection (211), causing a decrease

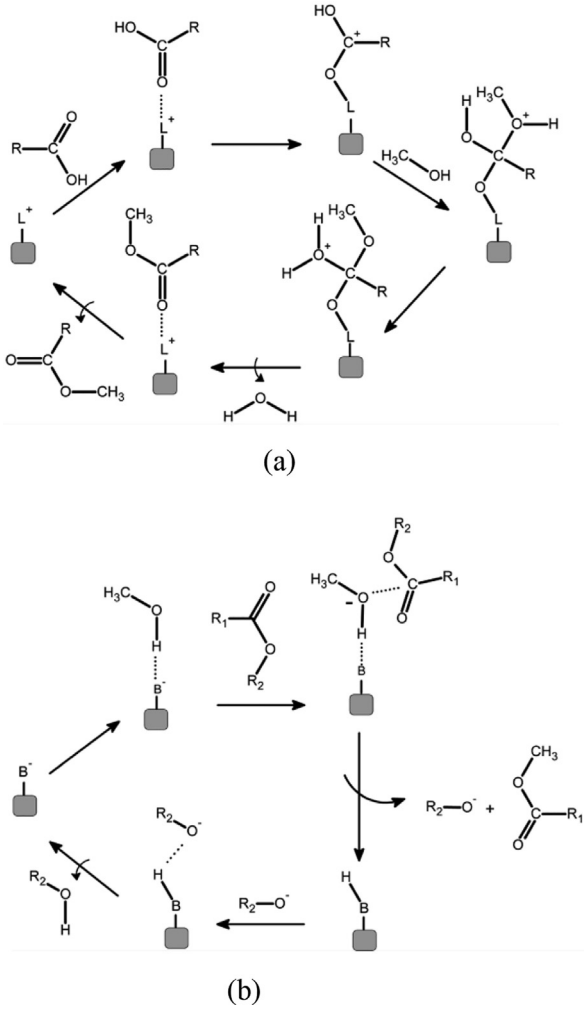

Fig. 1 (a) Esterification mechanism for heterogeneous catalysis. "L" represents the Lewis acid site and "R" the fatty acid radical; (b) Transesterification mechanism for heterogeneous catalysis. "B" represents the Lewis basic site, "R" and "R1" are radicals (Cordeiro et al, 2011).

both in the interplanar distance ($d_{2\ 1\ 1}$) and in the unit cell parameter (a_0). Liu et al. (2016) assign the raise of a_0 to tetrahedrically coordinated molybdenum atoms on the structure of the molecular sieve because the length of Mo—O—Si bonds is greater than those of Si—O—Si bonds.

4.1.3. Fourier transformed infrared spectroscopy

FTIR spectra of KIT-6 catalyst precursor and *x*_Mo-KIT-6 catalysts are shown in Fig. 5, in which the bands at 3391 and 1638 cm^{-1} correspond to the (—OH) stretching (*v*) vibration of adsorbed water molecules. All samples display five absorption peaks at about 1056, 963, 800, 565 e 442 cm^{-1}. These peaks for the catalytic precursor KIT-6 are attributed to the asymmetrical stretching of the Si—O—Si groups, the stretching of the oxygen atoms in the silanol Si—OH bonds, the symmetrical stretching of the Si—O—Si, the siloxane groups, Si—O stretching and the bending vibration of the Si—O—Si groups (Wawrzyńczak et al., 2021; Zhou et al., 2020). For the catalysts, the peaks in the 500–1000 cm^{-1} region

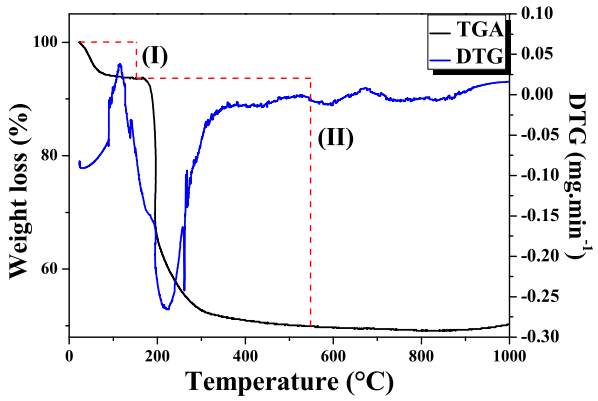

Fig. 2 Thermogravimetric (TG) analysis of the KIT-6 molecular sieve uncalcined.

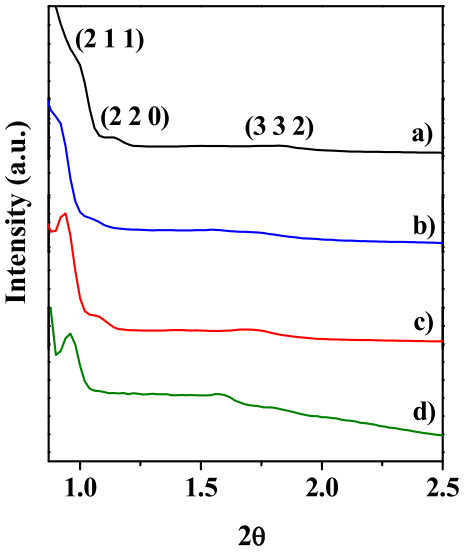

Fig. 3 Diffractograms of the (a) molecular sieve KIT-6 and of the catalysts (b) 30_Mo-KIT-6, (c) 20_Mo-KIT-6, and (d) 10_Mo-KIT-6.

are attributed to different stretching vibrations of Mo—O. For the 10_Mo-KIT-6 catalyst, it is possible to observe a band at 915 cm^{-1} that indicates the tetrahedrally coordinated Mo bond in the molecular sieve structure through the Mo—O—Si bond (Figueiredo et al., 2021; Rakngam et al., 2021).

4.1.4. Textural analysis by nitrogen adsorption (BET)

N_2 adsorption–desorption isotherms of the KIT-6 molecular sieve and the *x*_Mo-KIT-6 catalysts are presented in Fig. 6.

Fig. 6 (a, b, c) presents type IV adsorption isotherms with three distinct regions. The first one, for $P/P_0 < 0.6$, is related to N_2 adsorption on the monolayer, where there are micropores; the second one, corresponding to the interval between $0.6 < P/P_0 < 0.8$, presents a pronounced inflection characteristic of capillary condensation at the mesopores; the third one, for $P/P_0 > 0.9$, is assigned to the adsorption at the particle external surface multilayers (Leofanti et al., 1998; Zhou et al., 2020).

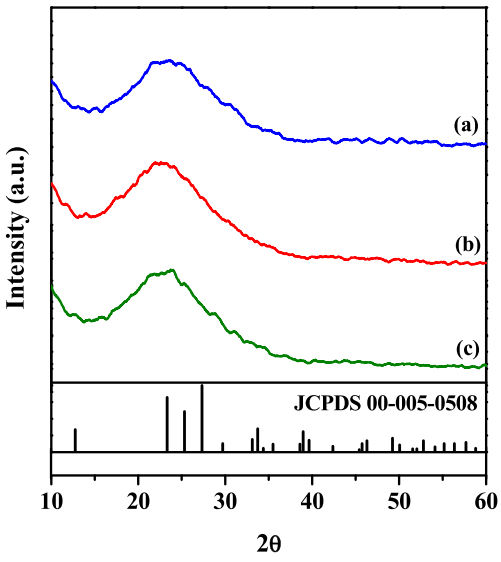

Fig. 4 Diffractograms of the catalysts (a) 30_Mo-KIT-6, (b) 20_Mo-KIT-6, and (c) 10_Mo-KIT-6.

From the desorption isotherms, it is possible to see that the support and the catalysts formed different "loops" of hysteresis with type H1 characteristics (Fig. 6 a, b, c), being the interval between $0.6 < P/P_0 < 0.8$ associated to capillary condensation which occurs both inside the mesopores with different regular sizes and in the cylindric pores system. In the interval between $0.4 < P/P_0 < 1$ (Fig. 6d) a mixed H1 and H3 type of hysteresis loop can be noticed. H3 hysteresis is usually found in solids derived from particle aggregates which develop different geometry pores (Cychosz and Thommes, 2018; Delitala et al., 2009; Hernando et al., 2018; Li et al., 2020b).

Fig. 7 shows the pore size distribution of the molecular sieve KIT-6 and *x*_Mo-KIT-6 catalysts.

It can be seen in Fig. 7 (a, b, c) that the KIT-6 molecular sieve and the 30_Mo-KIT-6 and the 20_Mo-KIT-6 catalysts present unimodal pore size distributions on the range of mesopores with central peaks of 33 Å, 33.23 Å and 39.40 Å. 10_Mo-KIT-6 (Fig. 7d) catalyst presented bimodal pore size distribution on the range of micro and mesopores, with peaks of 19.24 Å and 39.45 Å.

Textural properties of the KIT-6 molecular sieve and *x*-_Mo_KIT-6 catalysts are shown in Table 3. It can be seen that 10_Mo_KIT-6 presented a specific surface area 18% lower than the specific surface area of KIT-6 precursor. It can also be seen that the presence of molybdenum in the structure reduced both pore volume and pore diameter and increased the wall thickness. This is because molybdenum atomic radius is greater than Si atomic radius. In the process of direct synthesis Mo replaces Si in the structure of KIT-6. An exceeding concentration of the metal led to deformation of the Si—O—Si bonds due to longer length of Mo—O—Si bonds. The reduction in the specific surface area relative to KIT-precursor was lower for the other catalysts. For 20_Mo_KIT-6 catalyst, the molybdenum was incorporated directly in the crystal network, resulting greater formation of mesopores and bigger pore diameter. Textural properties reaffirm FTIR spectrometer analysis.

Table 2 Crystallographic parameters of the molecular sieve KIT-6 and of the catalysts 10_Mo-KIT-6, 20_Mo-KIT-6 and 30_Mo-KIT-6.

Sample	2θ	h k l	$d_{2\ 1\ 1}$ (Å)	a_0 (Å)
KIT-6	1.00	2 1 1	88.36	216.40
10_Mo-KIT-6	0.96	2 1 1	92.04	225.46
20_Mo-KIT-6	0.94	2 1 1	94.01	230.27
30_Mo-KIT-6	0.92	2 1 1	96.06	235.26

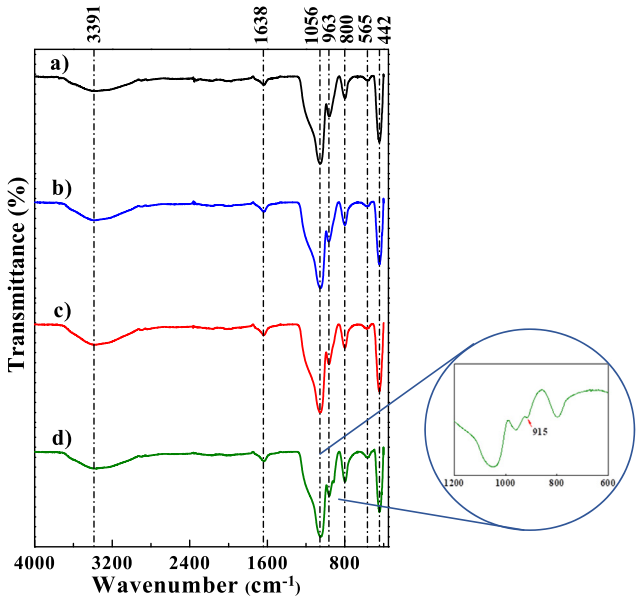

Fig. 5 FTIR spectra of the (a) molecular sieve KIT-6 and the catalysts (b) 30_Mo-KIT-6, (c) 20_Mo-KIT-6, and (d) 10_Mo-KIT-6.

4.2. Factors affecting the transesterification reaction

Table 4 shows fatty acid methyl ester (FAME) yield, density and acidity index of the biodiesel obtained. A high yield of FAME was observed for all conditions of reaction time and molybdenum content used in the experimental planning.

4.2.1. Effect of Si/Mo molar ratio

*x*_Mo-KIT-6 catalysts synthesized with different Si/Mo ratios (10, 20, 30) have been evaluated in the transesterification reaction. From Table 4 it is observed that the FAME yield is directly proportional to the molybdenum concentration in the catalyst structure.

Biodiesel yield increases with the increase of the metal concentration in the crystal structure both for oil/alcohol ratio 1/10 and 1/20. This result indicates that molybdenum in the structure had major influence in transesterification reaction. The amount of silicon species was not sufficient to bond with all molybdenum present, leading to exceeding metal agglomeration on the walls of the canals.

4.2.2. Effect of oil/alcohol ratio on biodiesel yield

Another important factor that influences transesterification reaction is the oil/alcohol ratio. It was observed that the

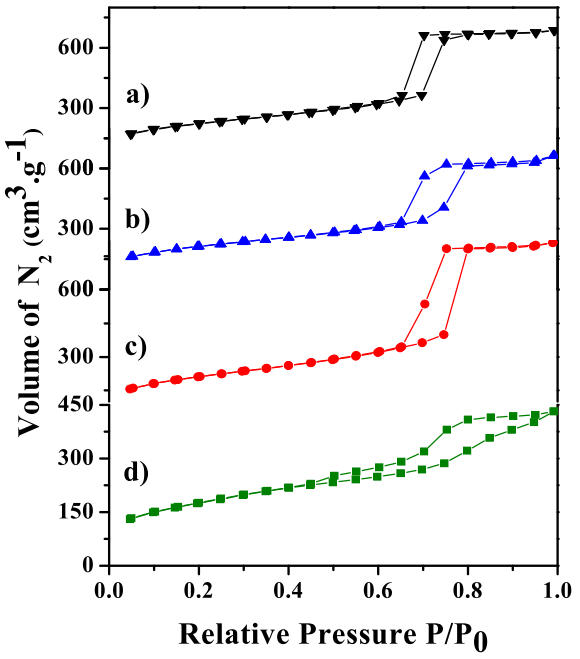

Fig. 6 N_2 adsorption/desorption isotherm of the molecular sieve (a) KIT-6 and of the catalysts (b) 30_Mo-KIT-6, (c) 20_Mo-KIT-6 and (d) 10_Mo-KIT-6.

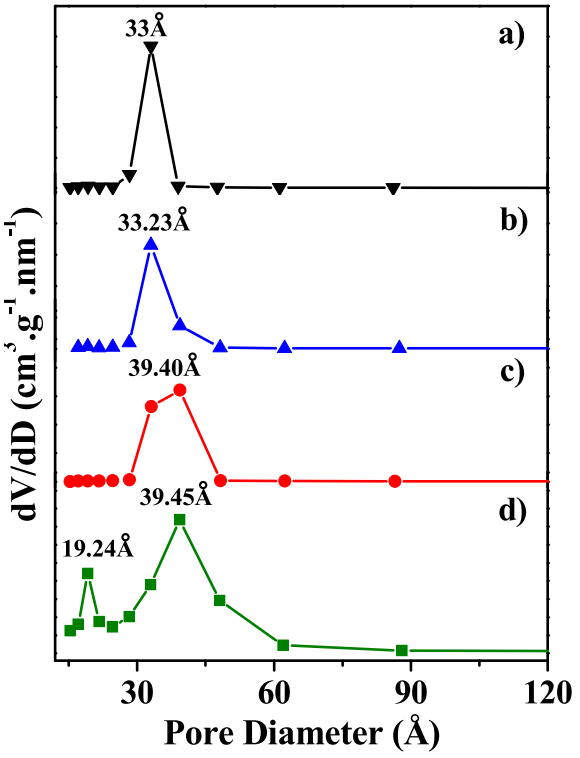

Fig. 7 Pore size distribution of the molecular sieve (a) KIT-6 and of the catalysts (b) 30_Mo-KIT-6, (c) 20_Mo-KIT-6, and (d) 10_Mo-KIT-6.

increase of alcohol content in reactional medium using 10_Mo-KIT-6 and 30_Mo-KIT-6 catalysts increased the methyl esters yield of about 16%. This raise is due to higher

Table 3 Textural properties of the catalytic precursor KIT-6 and of the catalysts *x*_Mo-KIT-6 (where *x*: Si/Mo = 10, 20 and 30).

Catalyst	S_{BET}[a] ($m^2.g^{-1}$)	S_{ext} ($m^2.g^{-1}$)	V_P^{micro} ($cm^3.g^{-1}$)	V_P^{mes} ($cm^3.g^{-1}$)	V_P[b] ($cm^3.g^{-1}$)	D_p[c] $_{BJH}$ (Å)	W_t[d] (Å)
KIT-6	759.56	572.07	0.12	0.95	1.07	33.05	75.15
10_Mo-KIT-6	615.66	315.61	0.18	0.50	0.68	19.17	93.56
20_Mo-KIT-6	736.62	641.91	0.07	1.19	1.26	39.40	75.74
30_Mo-KIT-6	731.74	503.16	0.14	0.89	1.03	33.02	84.60

[a] Specific surface area determined by Brunauer-Emmett-Teller (BET) method.
[b] Total pore volume recorded at $P/P_0 = 0.993552$.
[c] Pore diameter calculated by Barrett-Joyner-Halenda (BJH) method.
[d] Wall thickness (Å) = $(a_0/2) - D_p$.

Table 4 Experimental and predicted data of FAME yield, density and acidity index of the obtained oils.

Run	Factors		FAME yield (wt. %)			Density (kg m^{-3})	Acidity Index (mg KOH g^{-1})
	Si/Mo	Oil/alcohol	Exp.[a]	Pred.[b]	Res.[c]		
1	10	1/20	68.51	63.84	−4.67	893.7	1.31
2	30	1/20	44.43	41.30	−3.13	903.0	0.98
3	10	1/10	59.17	63.84	4.67	893.7	1.31
4	30	1/10	38.18	41.3	3.12	902.4	1.31
5	20	1/15	60.68	52.57	−8.11	897.8	1.07
6	20	1/15	58.56	52.57	−5.99	894.3	1.07
7	20	1/15	62.61	52.57	−10.04	895.6	1.47
Soybean oil						920	0.00

[a] Experimental values of response.
[b] Predicted values of response.
[c] Residual.

methanol content which shifts the reaction equilibrium towards FAMEs products (Gopinath et al., 2017). Methanol also diminishes the mixture viscosity and favors glycerin solubility which is a subproduct that might stress reaction equilibrium and, consequently, decrease the yield of FAMEs. For 1/15 ratio it is possible to see that esters yield on the presence of 20_Mo-KIT-6 catalyst is within the interval obtained with higher metal concentration catalyst (10_Mo-KIT-6) using lesser amounts of methanol. This fact might be assigned to the crystal and textural properties presented by the catalyst.

4.2.3. Chemical composition of FAME

The produced biodiesel composition is given in Table 5, the chromatograms shown in Fig. 8 and C_{FAMEi} wt.% was calculated from Eq.(3). The most commonly found fatty acids in biodiesel samples are: oleic (C18:1) followed by stearic (C18:0), linoleic (C18:2), palmitic (C16:0) and linolenic (C18:3) (Wan Ghazali et al., 2015). In all samples of biodiesel obtained, the predominant fatty acids were: polyunsaturated fatty acids, linoleic (C18:2; 49–54%) and linolenic (C18:3; 5–7%); unsaturated fatty acids, oleic acid (C18:1; 20–23%) and saturated fatty acids, palmitic acid (C16:0; 9–13%) and stearic (18:0; 2–3%). Soybean oil for biodiesel production has the following typical composition (Singh et al., 2019): oleic (20–30%), linoleic (50–60%), palmitic (6–10%), stearic (2–5%) and linolenic (5–11%). Thus, the biodiesel produced in this work 'has a typical composition of biodiesel from soybean reported in the literature (Singh et al., 2019; Tercini et al., 2018).

Table 5 Concentrations of $FAME_i$ in the biodiesel.

Biodiesel sample	C_{FAMEi} (wt.%)					
	(C16:0)	C (18:0)	(C18:1)	(C18:2)	(C18:3)	Others
1	11.54	2.80	22.68	54.34	7.04	1.60
2	12.32	2.98	22.86	53.74	7.01	1.09
3	11.48	2.81	22.31	53.29	6.87	3.24
4	12.35	3.08	22.75	53.51	7.06	1.25
5	11.16	2.54	21.53	51.07	6.98	6.72
6	11.04	2.52	21.40	50.93	6.81	7.30
7	11.09	3.03	21.41	51.45	6.96	6.06

4.2.4. Density and acidity level

Density and acidity level are important properties for the characterization of methyl or ethyl esters. According to EN ISO 367/12185 (ASTM D1298) and EN 14104 (ASTM D664) standards, biodiesel should have density within 50–900 kg/m^3 and acidity index below 0.5 mg KOH/g (Atabani et al., 2013; Singh et al., 2019).

Table 4 shows data of density and acidity values obtained via characterization of transesterified oils. For tests which used the 30_Mo-KIT-6 catalyst, density measurements are not in compliance with stablished standards because these essays resulted in the smallest yields in FAME in such a way that there was still a high concentration of non-converted triglycerides what elevated the sample density for presenting bigger

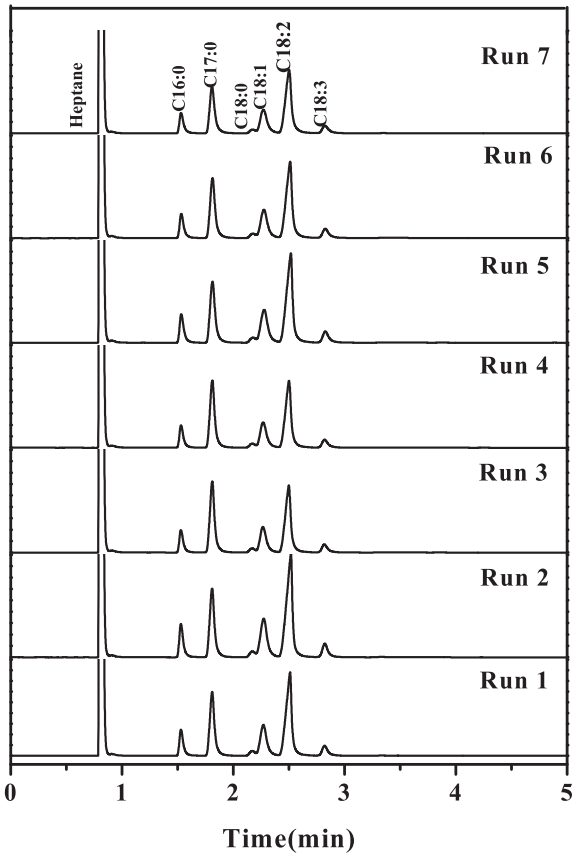

Fig. 8 Biodiesel samples chromatograms (Acronym: C16:0 – methyl palmitate; C17:0 – methyl heptadecanoate (internal standard); C18:0 – methyl stearate; C18:1 – methyl oleate; C18:2 – methyl linoleate; C18:3 – methyl linoleneate).

and consequently more dense molecules (Knothe and Razon, 2017). Regarding to the acidity level, results were outside stablished limits what might be associated to the high contents of free fatty acids and molybdenum leaching to the reaction medium, once this molecule has high acidity index (Bail et al., 2013).

4.3. Statistical data analysis

In order to evaluate the effects of indepent variables oil/alcohol ratio (A) and Si/Mo ratio (B) on the resulting variable (ester content), statistical treatment of data was done using

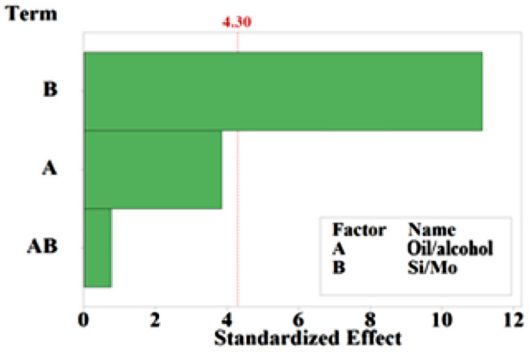

Fig. 9 Pareto Chart of the Standardized Effects ($\alpha = 0.05$).

Minitab 17.0® software at 5% ($\alpha = 0.05$) significance level. Table 6 shows the results from the analysis of variance (ANOVA).

Analyzing the P values in Table 6 (ANOVA), it can be observed that $\alpha \leq 0.05$ for factor B. This means that this factor has significance and influences the biodiesel yield. Another statistical parameter that reaffirms this result is the test F, once the value of F_{cal} for the same factor is bigger than the value of F_{tab}. The curve test was also realized comparing the values of F_{cal} and F_{tab}. It was observed that there was curvature at the evaluated region and the adopted model is quadratic for both catalysts. The determination coefficient (R^2) shows the model with 98.81% of significance and the correlation coefficient (R) indicated strong relationship among the data.

The Pareto chart shown in Fig. 9 shows the significance of factors on the transesterification reaction with confidence interval of 95%. The only factor which presented influence on the response variable was the Si/Mo molar ratio. This result supports the yields for esters given in Table 4, seen that the oil/alcohol ratio was smaller than the Si/Mo ratio used.

The contour graph shown in Fig. 10a evidences that biggest conversion values were observed on the left and right extremities at superior and inferior parts, under optimized conditions of Si/Mo ratio = 14.5 and oil/alcohol ratio = 20.92. These conditions led to yield results for methyl esters greater than 68.51%.

The response surface in Fig. 10b shows a curvature on the region of maximum yield for methyl esters what confirms data from Table 6 and Fig. 10a. The quadratic aspect can be explained through the effect of interactions between the independent variables Si/Mo and alcohol/oil. The desirability

Table 6 ANOVA for the experimental planning $2^2 + 3$ CtPt.

Source	Degree of freedom	Sum of squares	Mean Square	P-Value	F-Value	Tabulated F-Value	Remarks
A	1	60.76	60.76	0.06	14.81	18.51	Insignificant
B	1	507.83	507.83	0.01	123.75	18.51	Significant
AxB	1	2.39	2.39	0.52	0.58	18.51	Insignificant
Curvature	1	110.93	110.93	0.03	27.03	18.51	Significant
Error	2	8.21	4.10	–	–	–	–
Total	6	690.11	–		–	–	–
$R^2 = 98.81\%$			R = 9.94				

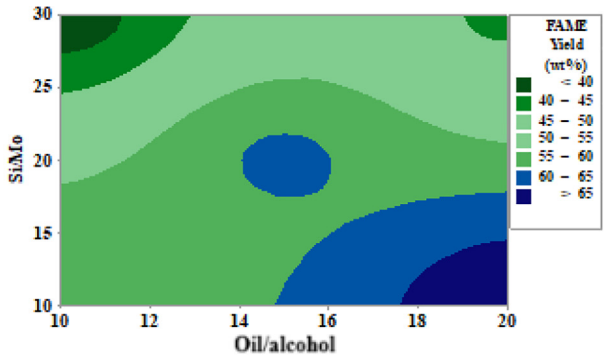

(a)

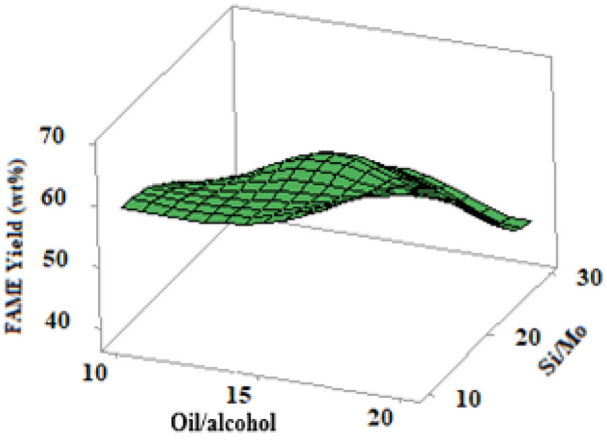

(b)

Fig. 10 Effect of the oil/alcohol and the Si/Mo ratios on biodiesel yield: (a) 2D contour plot; (b) 3D response surface.

function (D) is equal to 1, thus this function value can be understood as excellent.

The coded model which associates the yield of methyl esters to the independent variables is presented on Eq. (4).

$$Y = 52.57 + 3.90A - 11.27B - 0.77A * B + 8.04CtPt \quad (4)$$

Among the factors and interactions studied on the model for *x*_Mo-KIT-6 catalysts on Eq. (4), the Si/Mo factor (B) and the AxB interaction presented opposite effects, with smaller association between the data or individual factors. Variable B presents antagonistic effect, what means that there is greater interaction when compared to the sum of its individual effects or in an interactive way. This equation shows how individual factors or the interaction among them affect the yield (%) of soybean transesterification reaction. On the equation, single factor coefficients indicate the influence of the factor specifically while double factor coefficients and first order terms indicate the interaction between two factors and quadratic effects respectively. A positive sign represents a synergic effect, while a negative sign represents an antagonistic effect.

The cube plot in Fig. 11 shows the interactions between the factors. The greatest value is 68.51, presented when the 10_Mo-KIT-6 catalyst is used and the oil/alcohol ratio is

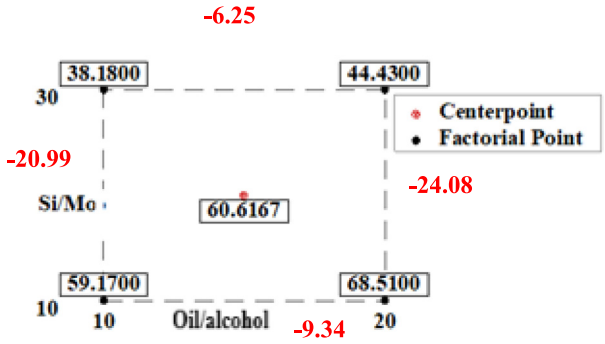

Fig. 11 Cube Plot (fitted means) for FAME Yield (%).

1/20. Main effects means for Si/Mo ratio and alcohol/oil ratio are 7.79 and 22.53 respectively. The main effect resulting mean (Si/Mo) has shown an increase of about 35% on the yield of methyl esters when compared to the alcohol/oil effect.

4.4. Comparison to literature

In this study, the maximum methyl esters yield was obtained at reactional conditions of the central point, suggesting that textural properties contribute to the catalytic performance in parallel to molybdenum concentration. The biodiesel yield varied from 44.43 to 68.51 wt%. Chen et al. (2020) used x_MoO_3/Naβ as catalyst to produce biodiesel from rice bran oil at different reactional conditions, and obtained a conversion in the range of 44.0–74.8 %. Biodiesel was produced from esterification of free fatty acid by Mohebbi et al. (2020) using MoO_3 incorporated to B-ZSM-5 as catalyst, and a conversion of up to 98% wt.% was obtained using 25_MoO_3/B-ZSM-5 at 160 oC for 6 h of reaction. Figueiredo et al. (2021) produced biodiesel from soybean oil using x_MoO_3/Al-SBA-15 catalysts, and a biodiesel yield of up to 98% was obtained with 10_MoO_3/Al-SBA-15 catalyst for 3 h of reaction at 150 oC.

5. Conclusion

The biodiesel was obtained in this study from soybean oil using a new heterogenous catalyst, produced from the incorporation of MoO3 in KIT-6 precursor. The yield obtained with this new catalyst is of the same magnitude of yield reported in the literature with different catalysts. ANOVA statistical analysis shows the molar ratio Si/Mo as the most significant variable for methyl ester yield. The factorial design showed that the optimum point for the yield of methyl esters (68.51%) was using the 10_Mo-KIT-6 catalyst, oil/alcohol ratio of 1/20 at 150 °C for 3 h. For the 1/15 oil/alcohol ratio, the yield of methyl esters in the presence of the 20_Mo-KIT-6 catalyst are in the range of methyl ester yield in the presence of the 10_Mo-KIT-6 catalyst, however using a lower amount of methanol, which means that the reaction conditions of the central point is the most suitable. Finally, Mo-KIT-6 catalyst demonstrated competitive potential to be used as catalyst for biodiesel production, and may be substitute homogeneous catalyst in a near future.

Funding

This work was supported by the National Council for Scientific and Technological Development (CNPq) and the Coordination for the Improvement of Higher Level Education a Personnel (CAPES).

Declaration of Competing Interest

The authors declare that they have no known competing financial interests or personal relationships that could have appeared to influence the work reported in this paper.

Acknowledgement

This research was supported by the Department of Chemical Engineering – Federal University of Campina Grande.

References

Ali, I., Saleh, T.A., 2020. Zeolite-graphene composite as support for molybdenum-based catalysts and their hydrodesulfurization performance. Appl. Catal. A Gen. 598. https://doi.org/10.1016/j.apcata.2020.117542.

Arrais Gonçalves, M., Karine Lourenço Mares, E., Roberto Zamian, J., Narciso da Rocha, G., Filho, Rafael Vieira da Conceição, L., 2021. Statistical optimization of biodiesel production from waste cooking oil using magnetic acid heterogeneous catalyst MoO3/SrFe2O4. Fuel 304. https://doi.org/10.1016/j.fuel.2021.121463.

Atabani, A.E., Silitonga, A.S., Anjum, I., Mahlia, T.M.I., Masjuki, H. H., Mekhilef, S., 2012. A comprehensive review on biodiesel as an alternative energy resource and its characteristics. Renew. Sustain. Energy Rev. 16, 2070–2093. https://doi.org/10.1016/j.rser.2012.01.003.

Atabani, A.E., Silitonga, A.S., Ong, H.C., Mahlia, T.M.I., Masjuki, H.H., Badruddin, I.A., Fayaz, H., 2013. Non-edible vegetable oils: A critical evaluation of oil extraction, fatty acid compositions, biodiesel production, characteristics, engine performance and emissions production. Renew. Sustain. Energy Rev. 18, 211–245. https://doi.org/10.1016/j.rser.2012.10.013.

Athar, M., Zaidi, S., 2020. A review of the feedstocks, catalysts, and intensification techniques for sustainable biodiesel production. J. Environ. Chem. Eng. 8,. https://doi.org/10.1016/j.jece.2020.104523 104523.

Bail, A., dos Santos, V.C., de Freitas, M.R., Ramos, L.P., Schreiner, W.H., Ricci, G.P., Ciuffi, K.J., Nakagaki, S., 2013. Investigation of a molybdenum-containing silica catalyst synthesized by the sol-gel process in heterogeneous catalytic esterification reactions using methanol and ethanol. Appl. Catal. B Environ. 130–131, 314–324. https://doi.org/10.1016/j.apcatb.2012.11.009.

Bigi, F., Piscopo, C.G., Predieri, G., Sartori, G., Scotti, R., Zanoni, R., Maggi, R., 2014. Molybdenum-MCM-41 silica as heterogeneous catalyst for olefin epoxidation. J. Mol. Catal. A: Chem. 386, 108–113. https://doi.org/10.1016/j.molcata.2014.01.028.

Cabrera-munguia, D.A., González, H., Gutiérrez-alejandre, A., Rico, J.L., Maya-yescas, R., Rosa, E., Huirache-acu, R., 2017. Heterogeneous acid conversion of a tricaprylin-palmitic acid mixture over Al-SBA-15 catalysts: Reaction study for biodiesel synthesis. Catal. Today 282, 195–203. https://doi.org/10.1016/j.cattod.2016.10.014.

Chen, C., Cai, L., Zhang, L., Fu, W., Hong, Y., Gao, X., Jiang, Y., Li, L., Yan, X., Wu, G., 2020. Transesterification of rice bran oil to biodiesel using mesoporous NaBeta zeolite-supported molybdenum catalyst: experimental and kinetic studies. Chem. Eng. J. 382, 122839. https://doi.org/10.1016/j.cej.2019.122839.

Chooi, C.Y., Sim, J.H., Tee, S.F., Lee, Z.H., 2021. Waste-derived green nanocatalyst for biodiesel production: kinetic-mechanism deduction and optimization studies. Sustainability 13, 5849. https://doi.org/10.3390/su13115849.

Chuah, L.F., Klemeš, J.J., Yusup, S., Bokhari, A., Akbar, M.M., 2016. A review of cleaner intensification technologies in biodiesel production. J. Cleaner Prod. 146, 181–193. https://doi.org/10.1016/j.jclepro.2016.05.017.

Cordeiro, C.S., Silva, F.R., Wypych, F., Ramos, L.P., 2011. Catalisadores heterogêneos para a produção de monoésteres graxos (biodiesel). Quim. Nova 34 (3), 477–486. https://doi.org/10.1590/S0100-40422011000300021.

Cychosz, K.A., Thommes, M., 2018. Progress in the physisorption characterization of nanoporous gas storage materials. Engineering 4, 559–566. https://doi.org/10.1016/j.eng.2018.06.001.

Dantas, J., Leal, E., Cornejo, D.R., Kiminami, R.H.G.A., Costa, A.C. F.M., 2020. Biodiesel production evaluating the use and reuse of magnetic nanocatalysts $Ni_{0.5}Zn_{0.5}Fe_2O_4$ synthesized in pilot-scale. Arab. J. Chem. 13, 3026–3042. https://doi.org/10.1016/j.arabjc.2018.08.012.

Delitala, C., Alba, M.D., Becerro, A.I., Delpiano, D., Meloni, D., Musu, E., Ferino, I., 2009. Synthesis of MCM-22 zeolites of different Si/Al ratio and their structural, morphological and textural characterisation. Microporous Mesoporous Mater. 118, 1–10. https://doi.org/10.1016/j.micromeso.2008.07.047.

Ewunie, G.A., Morken, J., Lekang, O.I., Yigezu, Z.D., 2021. Factors affecting the potential of Jatropha curcas for sustainable biodiesel production: a critical review. Renew. Sustain. Energy Rev. 137, 110500. https://doi.org/10.1016/j.rser.2020.110500.

Faba, E.M., Ferrero, G.O., Dias, J.M., Eimer, G.A., 2020. Na-Ce-modified-SBA-15 as an effective and reusable bimetallic mesoporous catalyst for the sustainable production of biodiesel. Appl. Catal. A Gen. 604. https://doi.org/10.1016/j.apcata.2020.117769.

Figueiredo, J.S.B., Alves, B.T.S., Freire, V.A., Alves, J.J.N., Barbosa, B.V.S., 2021. Preparation, characterization and evaluation of x-MoO3/Al-SBA-15 catalysts for biodiesel production. Mater. Renew. Sustain. Energy. https://doi.org/10.1007/s40243-021-00204-x.

Gopinath, S., Kumar, P.S.M., Arafath, K.A.Y., Thiruvengadaravi, K. V., Sivanesan, S., Baskaralingam, P., 2017. Efficient mesoporous $SO4^{2-}$/Zr-KIT-6 solid acid catalyst for green diesel production from esterification of oleic acid. Fuel 203, 488–500. https://doi.org/10.1016/j.fuel.2017.04.090.

Hosseinzadeh-Bandbafha, H., Tabatabaei, M., Aghbashlo, M., Khanali, M., Demirbas, A., 2018. A comprehensive review on the environmental impacts of diesel/biodiesel additives. Energy Convers. Manage. 174, 579–614. https://doi.org/10.1016/j.enconman.2018.08.050.

Hernando, H., Fermoso, J., Ochoa-Hernández, C., Opanasenko, M., Pizarro, P., Coronado, J.M., Čejka, J., Serrano, D.P., 2018. Performance of MCM-22 zeolite for the catalytic fast-pyrolysis of acid-washed wheat straw. Catal. Today 304, 30–38. https://doi.org/10.1016/j.cattod.2017.09.043.

Kleitz, F., Choi, S.H., Ryoo, R., 2003. Cubic Ia3d large mesoporous silica: synthesis and replication to platinum nanowires, carbon nanorods and carbon nanotubes. Chem. Commun. 3, 2136–2137. https://doi.org/10.1039/b306504a.

Kleitz, F., Yang, C.M., Thommes, M., 2007. Structural characterization and systematic gas adsorption studies on a series of novel ordered mesoporous silica materials with 3D cubic Ia-3d structure (KIT-6). In: Studies in Surface Science and Catalysis. Elsevier Masson SAS. https://doi.org/10.1016/S0167-2991(07)80289-8.

Knothe, G., Razon, L.F., 2017. Biodiesel fuels. Prog. Energy Combust. Sci. 58, 36–59. https://doi.org/10.1016/j.pecs.2016.08.001.

Krishnasamy, A., Bukkarapu, K.R., 2021. A comprehensive review of biodiesel property prediction models for combustion modeling studies. Fuel 302, 121085. https://doi.org/10.1016/j.fuel.2021.121085.

Leofanti, G., Padovan, M., Tozzola, G., Venturelli, B., 1998. Surface area and pore texture of catalysts. Catal. Today 41, 207–219. https://doi.org/10.1016/S0920-5861(98)00050-9.

Li, L., Yan, B., Li, H., Yu, S., Ge, X., 2020a. Decreasing the acid value of pyrolysis oil via esterification using ZrO2/SBA-15 as a solid acid catalyst. Renew. Energy 146, 643–650. https://doi.org/10.1016/j.renene.2019.07.015.

Li, R., Xue, T., Li, Z., Wang, Q., 2020b. Hierarchical structure ZSM-5/SBA-15 composite with improved hydrophobicity for adsorption-desorption behavior of toluene. Chem. Eng. J. 392, 124861. https://doi.org/10.1016/j.cej.2020.124861.

Liu, Q., Li, J., Zhao, Z., Gao, M., Kong, L., Liu, J., Wei, Y., 2016. Synthesis, characterization, and catalytic performances of potassium-modified molybdenum-incorporated KIT-6 mesoporous silica catalysts for the selective oxidation of propane to acrolein. J. Catal. 344, 38–52. https://doi.org/10.1016/j.jcat.2016.08.014.

Luna, M.D.G., Cuasay, J.L., Tolosa, N.C., Chung, T.W., 2017. Transesterification of soybean oil using a novel heterogeneous base catalyst: Synthesis and characterization of Na-pumice catalyst, optimization of transesterification conditions, studies on reaction kinetics and catalyst reusability. Fuel 209, 246–253. https://doi.org/10.1016/j.fuel.2017.07.086.

Manojkumar, N., Muthukumaran, C., Sharmila, G., 2020. A comprehensive review on the application of response surface methodology for optimization of biodiesel production using different oil sources. J. King Saud Univ. – Eng. Sci. https://doi.org/10.1016/j.jksues.2020.09.012.

Moraes, P.S., Igansi, A.V., Cadaval, T.R.S., Pinto, L.A.A., 2020. Biodiesel produced from crude, degummed, neutralized and bleached oils of Nile tilapia waste: production efficiency, physical-chemical quality and economic viability. Renew. Energy 161, 110–119. https://doi.org/10.1016/j.renene.2020.07.092.

Mukhtar, A., Saqib, S., Lin, H., Shah, M.U.H., Ullah, S., Younas, M., Rezakazemi, M., Ibrahim, M., Mahmood, A., Asif, S., Bokhari, A., 2022. Current status and challenges in the heterogeneous catalysis for biodiesel production. Renew. Sustain. Energy Rev. 157, 112012. https://doi.org/10.1016/j.rser.2021.112012.

Orege, J.I., Oderinde, O., Kifle, G.A., Ibikunle, A.A., Raheem, S.A., Ejeromedoghene, O., Okeke, E.S., Olukowi, O.M., Orege, O.B., Fagbohun, E.O., Ogundipe, T.O., Avor, E.P., Ajayi, O.O., Daramola, M.O., 2022. Recent advances in heterogeneous catalysis for green biodiesel production by transesterification. Energy Convers. Manage. 258, 115406. https://doi.org/10.1016/j.enconman.2022.115406.

Pinto, B.F., Garcia, M.A.S., Costa, J.C.S., de Moura, C.V.R., de Abreu, W.C., de Moura, E.M., 2019. Effect of calcination temperature on the application of molybdenum trioxide acid catalyst: Screening of substrates for biodiesel production. Fuel 239, 290–296. https://doi.org/10.1016/j.fuel.2018.11.025.

Rakngam, I., Osakoo, N., Wittayakun, J., Chanlek, N., Pengsawang, A., Sosa, N., Butburee, T., Faungnawakij, K., Khemthong, P., 2021. Properties of mesoporous Al-SBA-15 from one-pot hydrothermal synthesis with different aluminium precursors and catalytic performances in xylose conversion to furfural. Microporous Mesoporous Mater. 317, 110999. https://doi.org/10.1016/j.micromeso.2021.110999.

Rezania, S., Oryani, B., Park, J., Hashemi, B., Yadav, K.K., Kwon, E. E., Hur, J., Cho, J., 2019. Review on transesterification of non-edible sources for biodiesel production with a focus on economic aspects, fuel properties and by-product applications. Energy Convers. Manag. 201, 112155. https://doi.org/10.1016/j.enconman.2019.112155.

Sakthivel, A., Mahato, N.R., Baskaran, T., Christopher, J., 2015. Molybdenum carbonyl grafted onto silicate intercalated cobalt-aluminum hydrotalcite: a new potential catalyst for the hydroformylation of octene. Catal. Commun. 65, 55–61. https://doi.org/10.1016/j.catcom.2015.02.024.

Sakthivel, R., Ramesh, K., Purnachandran, R., Shameer, P.M., 2018. A review on the properties, performance and emission aspects of the third generation biodiesels. Renew. Sustain. Energy Rev. 82, 2970–2992. https://doi.org/10.1016/j.rser.2017.10.037.

Silva, C.A.A., Silva, C.F., Matos, J.M.E., 2018. Síntese, caracterização e aplicação do trióxido de molibdênio na fotocatálise de efluente têxtil sintético. Cerâmica 64, 454–465. https://doi.org/10.1590/0366-69132018643712341.

Singh, D., Sharma, D., Soni, S.L., Sharma, S., Kumari, D., 2019. Chemical compositions, properties, and standards for different generation biodiesels: a review. Fuel 253, 60–71. https://doi.org/10.1016/j.fuel.2019.04.174.

Tercini, A.C.B., Pinesi, M., Calera, G.C., Sequinel, R., Hatanaka, R. R., Oliveira, J.E., Flumignan, D.L., 2018. Ultrafast gas chromatographic method for quantitative determination of total FAMEs in biodiesel: an analysis of 90 s. Fuel 222, 792–799. https://doi.org/10.1016/j.fuel.2018.03.008.

Thoai, D.N., Photaworn, S., Kumar, A., Prasertsit, K., Tongurai, C., 2017. A novel chemical method for determining ester content in biodiesel. Energy Procedia 138, 536–543. https://doi.org/10.1016/j.egypro.2017.10.156.

Uchagawkar, A., Ramanathan, A., Hu, Y., Subramaniam, B., 2020. Highly dispersed molybdenum containing mesoporous silicate (Mo-TUD-1) for olefin metathesis. Catal. Today 343, 215–225. https://doi.org/10.1016/j.cattod.2019.03.073.

Wan Ghazali, W.N.M., Mamat, R., Masjuki, H.H., Najafi, G., 2015. Effects of biodiesel from different feedstocks on engine performance and emissions: a review. Renew. Sustain. Energy Rev. 51, 585–602. https://doi.org/10.1016/j.rser.2015.06.031.

Wawrzyńczak, A., Jarmolińska, S., Nowak, I., 2021. Nanostructured KIT-6 materials functionalized with sulfonic groups for catalytic purposes. Catal. Today. https://doi.org/10.1016/j.cattod.2021.06.019.

Wong, K.Y., Ng, J.H., Chong, C.T., Lam, S.S., Chong, W.T., 2019. Biodiesel process intensification through catalytic enhancement and emerging reactor designs: a critical review. Renew. Sustain. Energy Rev. 116. https://doi.org/10.1016/j.rser.2019.109399.

Xie, W., Zhao, L., 2014. Heterogeneous CaO-MoO3-SBA-15 catalysts for biodiesel production from soybean oil. Energy Convers. Manag. 79, 34–42. https://doi.org/10.1016/j.enconman.2013.11.041.

Young, C.G., 2003. Molybdenum. In: Comprehensive Coordination Chemistry II. Elsevier, pp. 415–527. https://doi.org/10.1016/B0-08-043748-6/03033-4.

Zabeti, M., Wan Daud, W.M.A., Aroua, M.K., 2009. Activity of solid catalysts for biodiesel production: A review. Fuel Process. Technol. 90, 770–777. https://doi.org/10.1016/j.fuproc.2009.03.010.

Zhang, Y., Duan, L., Esmaeili, H., 2022. A review on biodiesel production using various heterogeneous nanocatalysts: operation mechanisms and performances. Biomass Bioenergy 158, 106356. https://doi.org/10.1016/j.biombioe.2022.106356.

Zhou, X., Zhao, H., Liu, S., Ye, D., Qu, R., Zheng, C., Gao, X., 2020. Engineering nano-ordered of Ni nanoparticles on KIT-6 for enhanced catalytic hydrogenation of nitrobenzene. Appl. Surf. Sci. 525, 146382. https://doi.org/10.1016/j.apsusc.2020.146382.